Sequential resonant tunneling in quantum cascade lasers

Romain Terazzi,* Tobias Gresch, Andreas Wittmann, and Jérôme Faist†
Quantum Optoelectronics Group, Institute for Quantum Electronics, ETH, 8086 Zürich, Switzerland
(Received 29 August 2008; published 31 October 2008)

A model of sequential resonant tunneling transport among two-dimensional subbands that takes into account explicitly elastic scattering is investigated. It is compared to transport measurements performed on quantum cascade lasers, where resonant tunneling processes are known to be dominating. Excellent agreement is found between experiment and theory over a large range of current, temperature, and device structures.

DOI: 10.1103/PhysRevB.78.155328 PACS number(s): 42.55.Px, 05.60.Gg, 52.25.Fi, 85.30.De

I. INTRODUCTION

Resonant tunneling in semiconductor heterostructures has motivated many experimental and theoretical studies. One of the most studied cases is the resonant tunneling diode, where a quantum well is formed by a double-barrier region.[1] Under a variable applied electric field, the transparency of the system is probed by coherent tunneling of electrons at the Fermi energy of the contact region.[2,3] The voltage-current curve exhibits a clear maximum when the emitter electrode aligns with a resonance of the well. This perfect case might be realized when the exit barrier is made so thin that the escape tunneling rate is much faster than other dephasing mechanisms. Because of strong in-plane scattering this condition is difficult to achieve. Usually current proceeds by sequential tunneling as it is the case in quantum cascade lasers.

In the pioneer work of Kazarinov, the current is expressed in a density matrix model, where the resonance curve is found Lorentzian with a homogeneous broadening given by the average value of elastic scattering matrix elements. Because of the averaging the electrons tunnel between subbands, conserving their in-plane wave vectors. More recently a refined model that includes previously averaged-out second-order mechanisms was developed.[4] Second-order scattering is known to yield gain without a net population inversion[5] through scattering assisted optical transitions, but it also affects more generally resonant tunneling by allowing transitions between subband states of different wave vectors.[4] It is found that resonant tunneling occurs with conservation of the energy rather than the wave vector, contrarily to the first-order case.[6]

In this paper we demonstrate the important role played by the second-order formulation of the current in sequential resonant tunneling and, therefore, in the carrier transport of semiconductor heterostructures.

II. SECOND-ORDER CURRENT

When second-order terms are considered in the calculation, the current density between a pair of subbands coupled through a barrier is expressed as[4,6]

$$\frac{j}{d} = e\Omega^2 \sum_k \frac{\gamma_k^1 (f_k^2 - f_{q_+}^1) + \gamma_k^2 (f_{q_-}^2 - f_k^1)}{\Delta^2 + (\gamma_k^1 + \gamma_k^2)^2} \tag{1}$$

with $q_\pm = \hbar^{-1}\sqrt{2m^*(\epsilon_k \pm \Delta)}$, where f_k^i is the carrier distribution in subband i at wave vector k, Δ is the detuning between the subband edges $\Delta = \epsilon_2 - \epsilon_1$, $\hbar\Omega$ is the coupling energy through the barrier, d is the difference between the two centroids of the wave functions $d = z_2 - z_1$, e is the elementary charge, and γ_k^i is the broadening of state i at wave vector k.

When a low density of electrons is distributed thermally in each subband, with the same electronic temperature T, and that a same and uniform scattering potential is considered ($\gamma_k^1 = \gamma_k^2 = \gamma$), the current density can be integrated and simply rewritten as

$$\frac{j}{d} = \frac{e\Omega^2 2\gamma}{\Delta^2 + (2\gamma)^2}\{\theta(\Delta)(n_2 - e^{-\beta\hbar|\Delta|}n_1) + \theta(-\Delta)(e^{-\beta\hbar|\Delta|}n_2 - n_1)\}, \tag{2}$$

where $\theta(x)$ is the Heaviside function, with $\theta(x^-) = 0$, $\theta(x^+) = 1$, and $\theta(0) = \frac{1}{2}$, $\beta = 1/kT$ with k the Boltzmann constant, and n_i is the net population of subband i.

The current density is no more driven by the population difference $n_2 - n_1$ but by an effective population term. We want to examine two extreme cases: equally populated subbands $n_2 = n_1 = n$ and one empty subband $n_1 = 0$. The first case is shown in Fig. 1(a). The current density is dispersive shaped around the resonance. A negative current peak occurs when the detuning is negative; this is when the edge of subband 1 is above the edge of subband 2. When the subbands are aligned the current is zero, and the first-order approximation is recovered. The current then turns to be positive after the edge of subband 2 has overcome the edge of subband 1; this is when the detuning is positive. The dispersive shape is the consequence of electron tunneling at a constant energy rather than at a constant wave vector. As shown in Fig. 1(a) the first-order model yield a zero current for any detuning. This case illustrates a superlattice: the current is zero until second-order scattering terms have been taken into account.

The case where one subband is empty is shown in Fig. 1(b). For negative detunings the current between the subbands is exponentially reduced as only the electrons with a sufficient kinetic energy are able to tunnel to subband 1. Contrarily, for positive detunings, the first- and second-order curves overlap perfectly as all electrons are above the edge of subband 1.

Generally the first-order model is recovered as the thermal energy largely overcomes the detuning energy $kT \gg \hbar|\Delta|$, as it is the case in Ref. 7. In Eq. (2), the exponential cutoff tends to one as the temperature tends to infinity, spreading electrons in a uniform distribution.

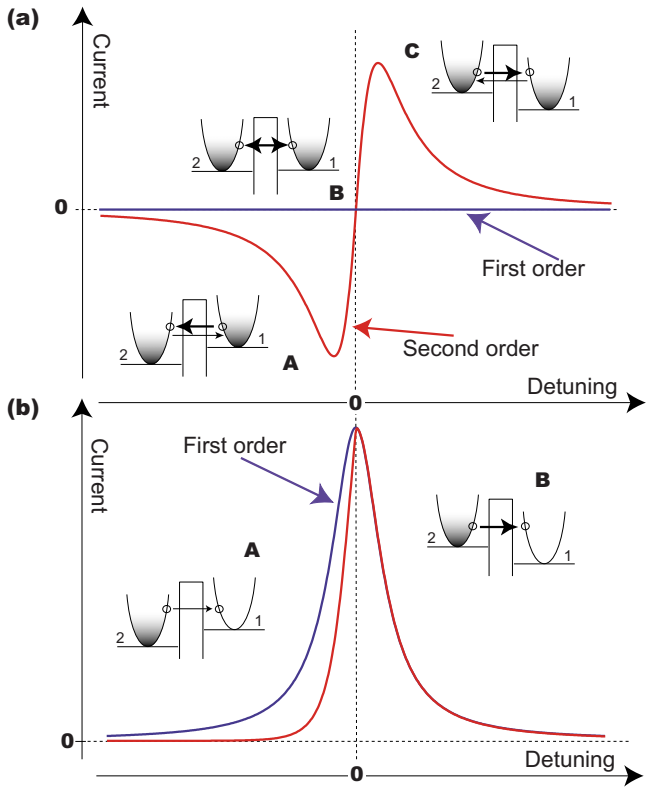

FIG. 1. (Color online) (a) Effects of second-order contributions on tunneling between a pair of equally populated subbands. (A) When the detuning is negative, the subband edge of subband 1 is above the edge of subband 2. As tunneling conserves energy, the current flow from 1 to 2 is greater than the current flow from 2 to 1, yielding a negative net current. (B) When the subbands are aligned, the detuning is zero and both contributions cancel, yielding a zero net current. (C) The detuning is positive and, therefore, the edge of subband 2 is above the edge of subband 1, yielding a positive net current between subbands. (b) Empty subband 1. (A) The current is reduced as only a fraction of electrons can tunnel. (B) Models overlap perfectly.

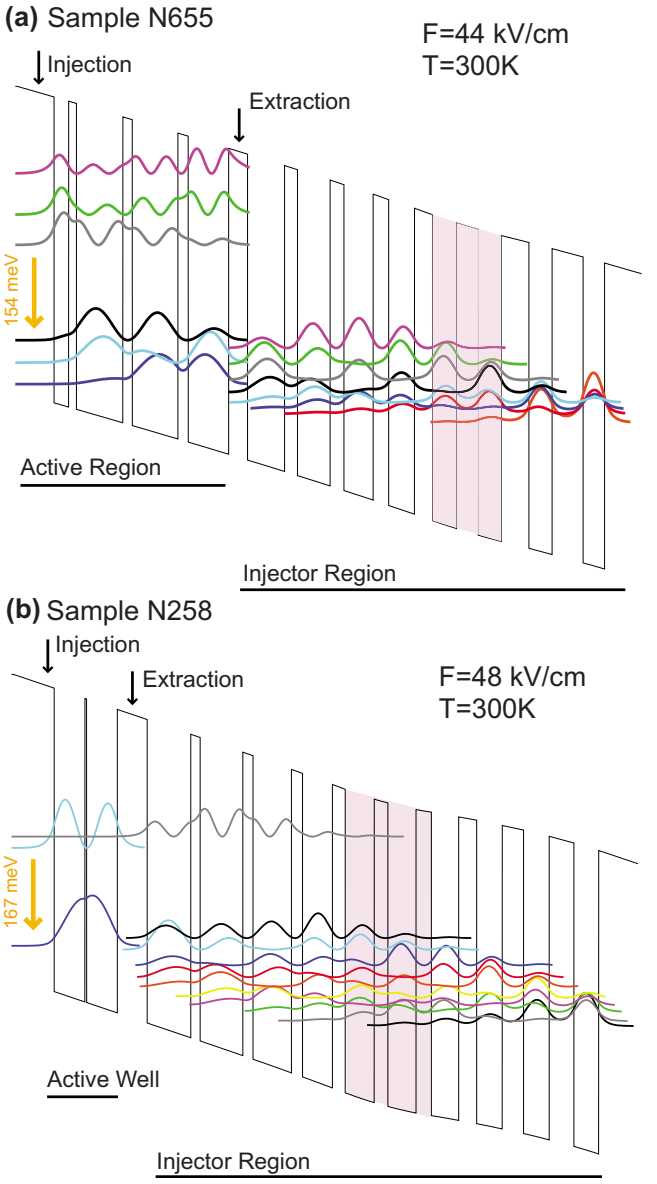

FIG. 2. (Color online) Each structure is shown at injection resonance field. The layer sequence starts from the injection barrier, and the thicknesses are in nm; roman and bold numbers indicate $In_{0.53}Ga_{0.47}As$ and $Al_{0.48}In_{0.52}As$ alloy, respectively, acting as well, resp. barrier material. (a) Layers: **4.3**/1.7/**0.9**/5.4/**1.1**/5.3/**1.2**/4.7/**2.2**/4.3/**1.5**/3.8/**1.6**/3.4/**1.8**/3.0/**2.1**/2.8/**2.5**/2.7/**3.2**/2.7/**3.6**/2.5. Underlined layers are 1.5×10^{17} cm^{-3} Si doped. Nominal sheet carrier density is 1.2×10^{11} cm^{-2}. Period length is 68.3 nm, repeated 35 times. The optical transition occurs at ≈154 meV. (b) Layers: **4.8**/3.6/**0.2**/3.6/**3.5**/5.1/**1.1**/5.0/**1.2**/4.5/**1.3**/3.5/**1.5**/3.4/**1.6**/3.3/**1.8**/3.2/**2.1**/3.0/**2.5**/3.0/**2.9**/2.9. Underlined layers are 3×10^{17} cm^{-3} Si doped. Nominal sheet carrier density is 3.03×10^{11} cm^{-2}. Period length is 68.6 nm, repeated 35 times. The optical transition occurs at ≈167 meV.

III. QUANTUM CASCADE LASERS

As second-order mechanisms strongly affect the resonant current between a pair of subbands, we aim to show its impact on more complex semiconductor heterostructures such as quantum cascade lasers.[8] We, therefore, have implemented second-order effects in the computation of the voltage-current characteristic.

The computational model is based on the density matrix, where dissipation is included as rate equations for the populations and as dephasing times for the polarizations. The precise implementation will be detailed somewhere else.[9] A typical quantum cascade laser is a repetition of a fundamental period as shown in Fig. 2. These periods are coupled through an injection barrier. Electrons are injected by sequential resonant tunneling from a period to the next one. The period itself can be separated in an active region, where the laser transition occurs, and an injector region, where carriers are relaxed before they are injected into the next period. For many structures and the ones presented here, the active region is coupled to the injector region through an extraction barrier as shown in Fig. 2. We, therefore, have implemented tight-binding and sequential resonant tunneling at the injection and at the extraction barrier. In the active region and the injection region, the carriers are relaxed through intersubband scattering. The mechanisms we have considered[10,11] in-

clude LO phonons, interface roughness, and ionized impurities (dopants) scattering. Nonparabolicity effects and self-consistency of the potential are accounted by the model. A uniform electronic temperature is computed for all subbands, based on the electron energy balance.[12] The numerical simulations output the populations of the subbands and the current density flowing through the heterostructure. We are, therefore, able to predict the voltage-current characteristic of a particular quantum cascade structure. In order to test the impact of second-order transport, we have implemented both first- and second-order sequential resonant tunneling models.

IV. RESULTS

We present two quantum cascade structures in different coupling regimes. The first (Sample N655) shown in Fig. 2(a) has a strong coupling between the active and the injector regions as the extraction barrier is made sufficiently thin (22 Å). Contrarily in Fig. 2(b) the second structure (Sample N258) is a single quantum well as its active region is formed by one well only, weakly coupled to the injector region by a thick extraction barrier (30 Å).

The current-voltage curves for both structures are shown in Fig. 3. The measurements are taken in continuous mode for low currents and in pulsed mode when current flow causes a heating of the sample. The cryostat temperature for the first sample (N655) is 300 K, while it is 80, 180, and 300 K for the second (N258).

In Fig. 3(a) the second-order voltage-current curve fits the experimental data much better than the first-order approximation from the very low currents to the maximal current.

If we focus on the low-field values of the voltage-current curve, the second-order model clearly better predicts the experimental behavior than the first-order model does. In particular it yields a zero net current at zero field, which is an important validation of the computational model.

The results for the single quantum well structure (N258) are shown in Fig. 3(b). We have shown simulated curves with second-order model only because the first-order model failed to converge at low-field value and is largely off from the measurements. Apart from a constant process-related serial resistance (0.5 Ω) that yields a systematically higher experimental bias, the model was able to reproduce nicely the experiment, in particular for high temperature where the transport in the structure is clearly dominated by optical phonons. The model predicts the low-temperature curve with less accuracy because the transport at such a temperature also require the computation of scattering rates due to acoustical phonons and electron-electron interactions, which are not computed in the present model.

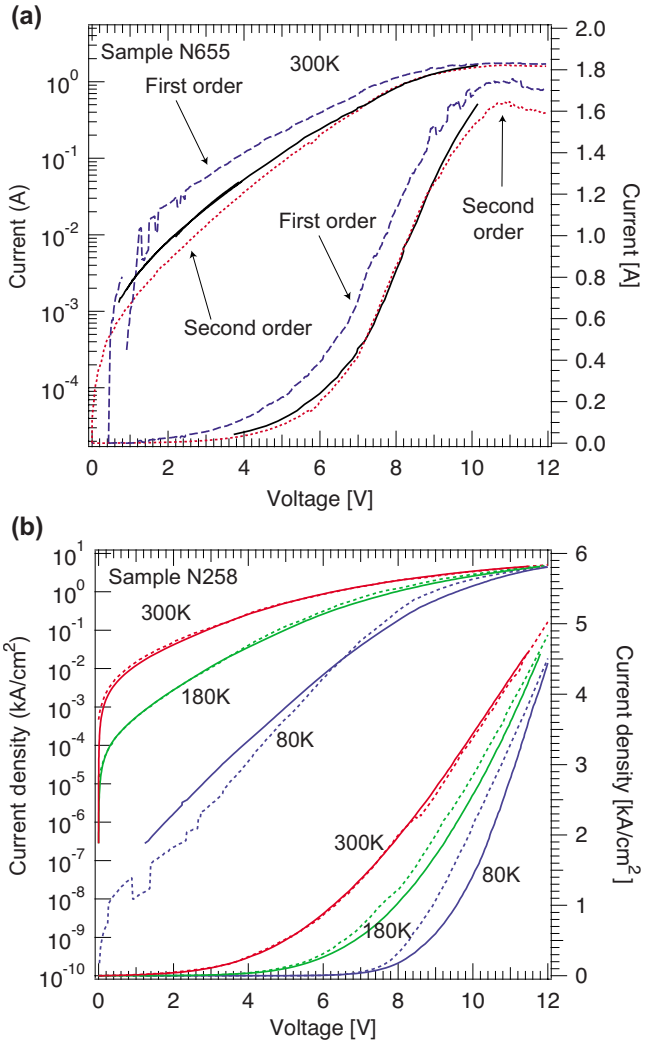

FIG. 3. (Color online) (a) Voltage-current characteristics; experimental data (full line), simulation with second-order resonant tunneling (dotted line), simulation with first-order model (dashed line). The current curves are shown both in log scale (left axis) for inspection of low currents and in linear scale (right axis) for inspection of the dynamic range. (b) Single quantum well current-voltage curves for three temperatures: 15, 180, and 300 K. Measurements displayed in full line. Simulation in dotted line.

V. CONCLUSION

Agreement between computed and experimental current-voltage characteristics has already been reported for other model approaches such as based on Monte Carlo,[13–15] scattering,[16,17] or nonequilibrium Green's functions;[18] this work aims to extend the comparison between theory and experiment to a larger range of currents, temperature, and structure design. Formally, the current driven by tunneling between two subbands through a barrier or by optical absorption are physically equivalent because both processes conserve the in-plane wave vector. As a result, the striking agreement between the predictions of the second-order model and the experiment can be interpreted as a strong experimental evidence for the validity of the Bloch gain model.

ACKNOWLEDGMENTS

This work was supported by the Swiss National Science Foundation, the National Center of Competence in Research, Quantum Photonics, and the Swiss Commission for Technology and Innovation.

*terazzi@phys.ethz.ch
†jerome.faist@phys.ethz.ch

[1] C. Rossel, P. Guéret, and H. Meier, J. Appl. Phys. **67**, 900 (1990).
[2] T. Ihn, H. Carmona, P. C. Main, L. Eaves, and M. Henini, Phys. Rev. B **54**, R2315 (1996).
[3] J. P. Eisenstein, T. J. Gramila, L. N. Pfeiffer, and K. W. West, Phys. Rev. B **44**, 6511 (1991).
[4] H. Willenberg, G. H. Döhler, and J. Faist, Phys. Rev. B **67**, 085315 (2003).
[5] R. Terazzi, T. Gresch, M. Giovannini, N. Hoyler, N. Sekine, and J. Faist, Nat. Phys. **3**, 329 (2007).
[6] A. Wacker, Adv. Solid State Phys. **41**, 199 (2001).
[7] R. Kazarinov and R. Suris, Sov. Phys. Semicond. **6**, 120 (1972).
[8] J. Faist, F. Capasso, D. Sivco, C. Sirtori, A. Hutchinson, and A. Cho, Science **264**, 553 (1994).
[9] R. Terazzi (unpublished).
[10] T. Unuma, M. Yoshita, T. Noda, H. Sakaki, and H. Akiyama, J. Appl. Phys. **93**, 1586 (2003).
[11] S. Tsujino, A. Borak, E. Müller, M. Scheinert, C. Falub, H. Sigg, D. Grützmacher, M. Giovannini, and J. Faist, Appl. Phys. Lett. **86**, 062113 (2005).
[12] P. Harrison, D. Indjin, and R. Kelsall, J. Appl. Phys. **92**, 6921 (2002).
[13] H. Callebaut and Q. Hu, J. Appl. Phys. **98**, 104505 (2005).
[14] R. C. Iotti and F. Rossi, Phys. Rev. Lett. **87**, 146603 (2001).
[15] H. Backe, M. Hies, H. Kunz, W. Lauth, O. Curtze, P. Schwamb, M. Sewtz, W. Theobald, R. Zahn, K. Eberhardt, N. Trautmann, D. Habs, R. Repnow, and B. Fricke, Phys. Rev. Lett. **80**, 920 (1998).
[16] K. Donovan, P. Harrison, and R. W. Kelsall, J. Appl. Phys. **89**, 3084 (2001).
[17] D. Indjin, P. Harrison, R. W. Kelsall, and Z. Ikonic, J. Appl. Phys. **91**, 9019 (2002).
[18] A. Wacker, Phys. Rev. B **66**, 085326 (2002).